Electronic Supplementary Material (ESI) for Chemical Science.

Surprising Solvent-Induced Structural Rearrangements in Large [N···I+···N] Halogen-Bonded Supramolecular Capsules: An Ion Mobility-Mass Spectrometry Study

Ulrike Warzok,[1] Mateusz Marianski,[2,‡] Waldemar Hoffmann,[1,2] Lotta Turunen,[3] Kari Rissanen,[3] Kevin Pagel,[1,2] and Christoph A. Schalley[1,*]

[1] Institut für Chemie und Biochemie, Freie Universität Berlin, Takustraße 3, 14195 Berlin, Germany
[2] Fritz-Haber-Institut der Max-Planck-Gesellschaft, Faradayweg 4-6, 14195 Berlin, Germany
[3] Department of Chemistry, NanoScience Center, University of Jyvaskyla, Department of Chemistry, P.O. Box 35, 40014 Jyväskylä, Finland

Supporting Information

Table of Content

1. General Information

Reagents were purchased from commercial suppliers and used without further purification. The hexyl-substituted ethylene-bridged tetrakis(4-pyridyl)cavitand **C_H**, the hexyl-substituted ethylene-bridged tetrakis(3-pyridyl)cavitand **C_D** and the *iso*-butyl-substituted ethylene-bridged tetrabromocavitand were prepared according to reported procedures.[1,2] ^{1}H and ^{13}C NMR spectra were recorded on a Bruker Avance III 500 or Avance 400 spectrometers. All signals are given as δ values in ppm using residual solvent signals as the internal standard. Coupling constants are given in Hz. Melting points were determined with melting point apparatus SMP3. Positive-mode electrospray ionization quadrupole-time-of-flight high resolution mass spectrometry (ESI-Q-TOF-HRMS) measurements were performed with a micromass LCT ESI-TOF instrument for analysis of *iso*-butyl-substituted ethylene-bridged tetrakis(4-pyridyl)cavitand.

2. Synthesis and Characterization

C_4-ethylene-bridged tetrakis(4-pyridyl)cavitand C_{H4}

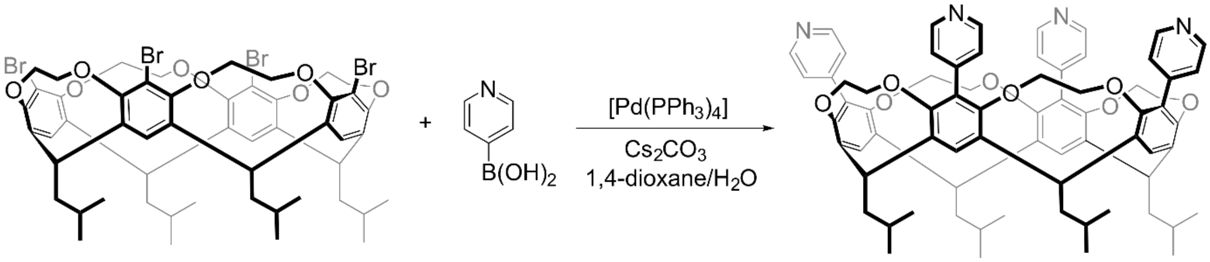

Scheme S1: Synthesis of ethylene-bridged tetrakis(4-pyridyl) cavitand.

The *iso*-butyl-substituted tetrakis(4-pyridyl)ethylenecavitand was synthesized according to a reported procedure.[1] To the flask containing *iso*-butyl-substituted ethylene-bridged tetrabromocavitand (500 mg, 420 µmol), pyridyl-4-boronic acid (270 mg, 2.2 mmol), [Pd(PPh$_3$)$_4$] (130 mg, 110 µmol) and Cs_2CO_3 (2.2 g, 6.6 mmol), degassed 1,4-dioxane (100 mL) and water (2.0 mL) were added under argon. The reaction mixture was degassed three times, then refluxed at 110 °C for 2 d. The mixture was cooled to room temperature and the solvent was evaporated under reduced pressure. The residue was dissolved in CH_2Cl_2 (70 mL) and water (70 mL) was added. After the phases were separated, the aqueous phase was extracted with CH_2Cl_2

(2 x 70 ml). The combined organic phases were dried over $MgSO_4$. The solvent was removed under reduced pressure to give the crude product, which was purified by column chromatography (SiO_2, CH_2Cl_2/MeOH 9:1). The product was obtained as a white solid (220 mg, 44 %). m.p. >270 ^{o}C (decomposition); ^{1}H NMR (500 MHz, $CDCl_3$, 303 K) δ (ppm): 1.00 (d, J = 6.8 Hz, 24H, CH_3), 1.40-1.48 (m, 4H, CH), 2.10-2.13 (m, 8H, CH_2), 3.40-3.43 (m, 8H, CH_{2in}), 3.86-3.90 (m, 8H, CH_{2out}), 5.41 (t, J = 8.0 Hz, 4H, CH), 7.10 (d, J = 5.4 Hz, 8H, pyr-H), 7.62 (s, 4H, Ar-H), 8.60 (d, J = 4.9 Hz, 8H, pyr-H)). ^{13}C NMR (126 MHz, $CDCl_3$, 303 K) δ (ppm): 22.8, 26.3, 31.6, 43.8, 72.4, 125.0, 125.2, 128.7, 136.4, 143.8, 149.4, 151.2; LCT ESI-TOF: found 1125.5751 $[M + H]^+$, calc. 1125.5736 $[M + H]^+$.

^{1}H and ^{13}C NMR spectra

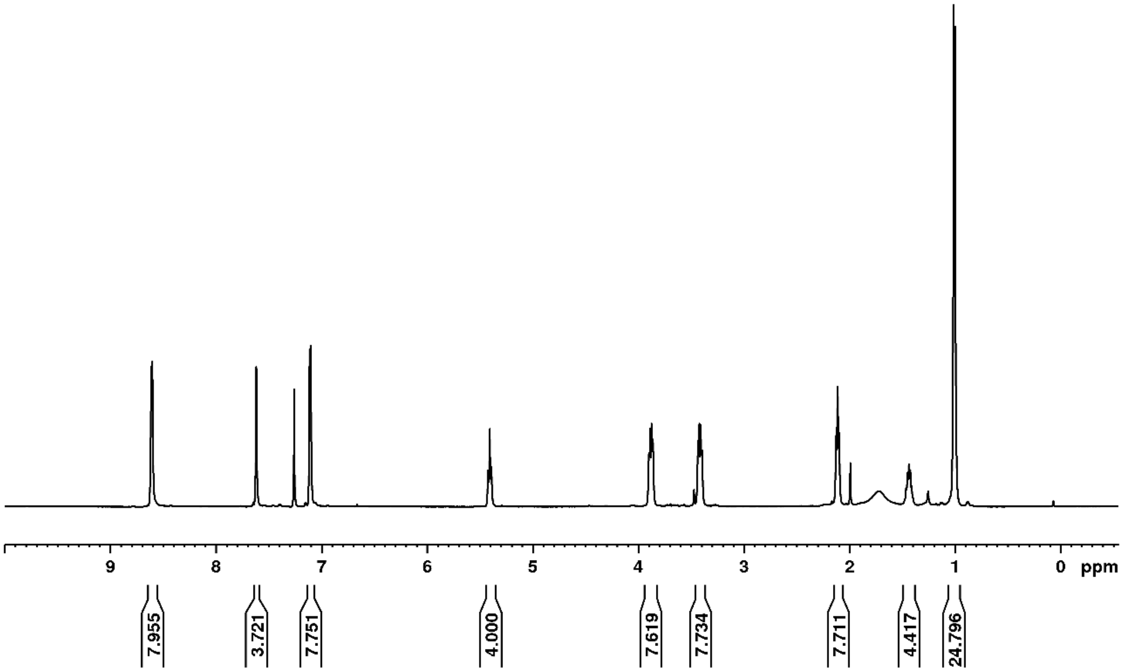

Figure S1: ^{1}H NMR spectrum of *iso*-butyl-substituted ethylene-bridged tetrakis(4-pyridyl)cavitand ($CDCl_3$, 303K, 400 MHz).

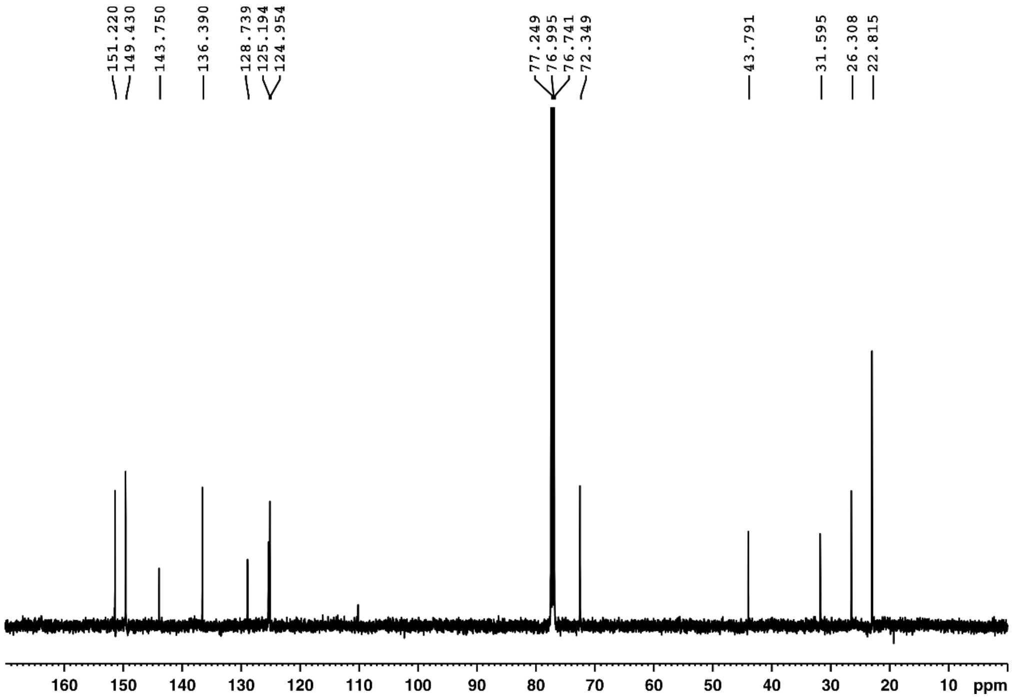

Figure S2: ^{13}C NMR spectrum of *iso*-butyl-substituted ethylene-bridged tetrakis(4-pyridyl)cavitand ($CDCl_3$, 303 K, 126 MHz).

3. Solvent-dependent Formation of Pentameric Capsules

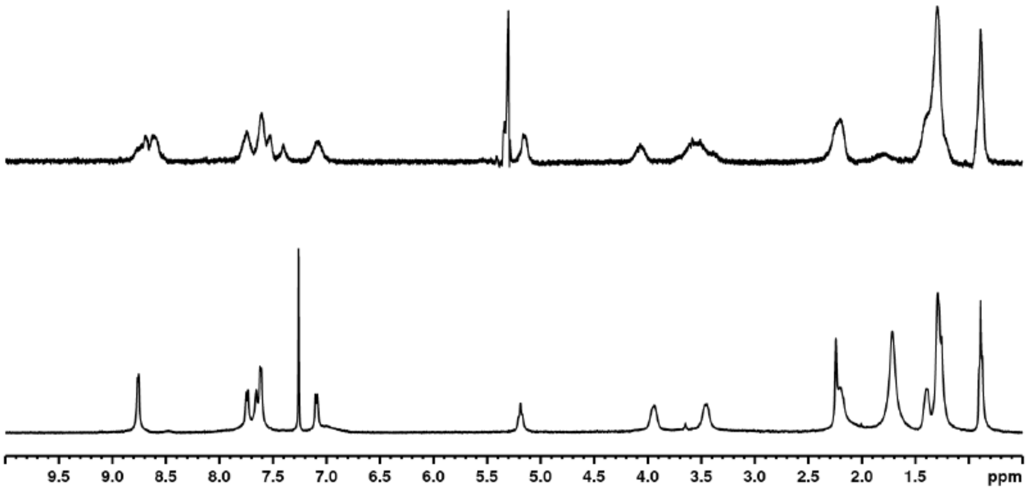

Figure S3: ^{1}H NMR spectra of halogen-bonded pentameric capsule **3** in CD_2Cl_2 (top) and hexameric capsule **2** in $CDCl_3$ (bottom, as previously published[2]). Clearly, both samples exhibit signals with similar chemical shifts. In contrast to the hexamer, which exhibits only one set of signals due to its high symmetry, the pentamer spectrum consists of several sets of signals in agreement with the presence of two different isomers each of which have a lower symmetry than the hexamer.

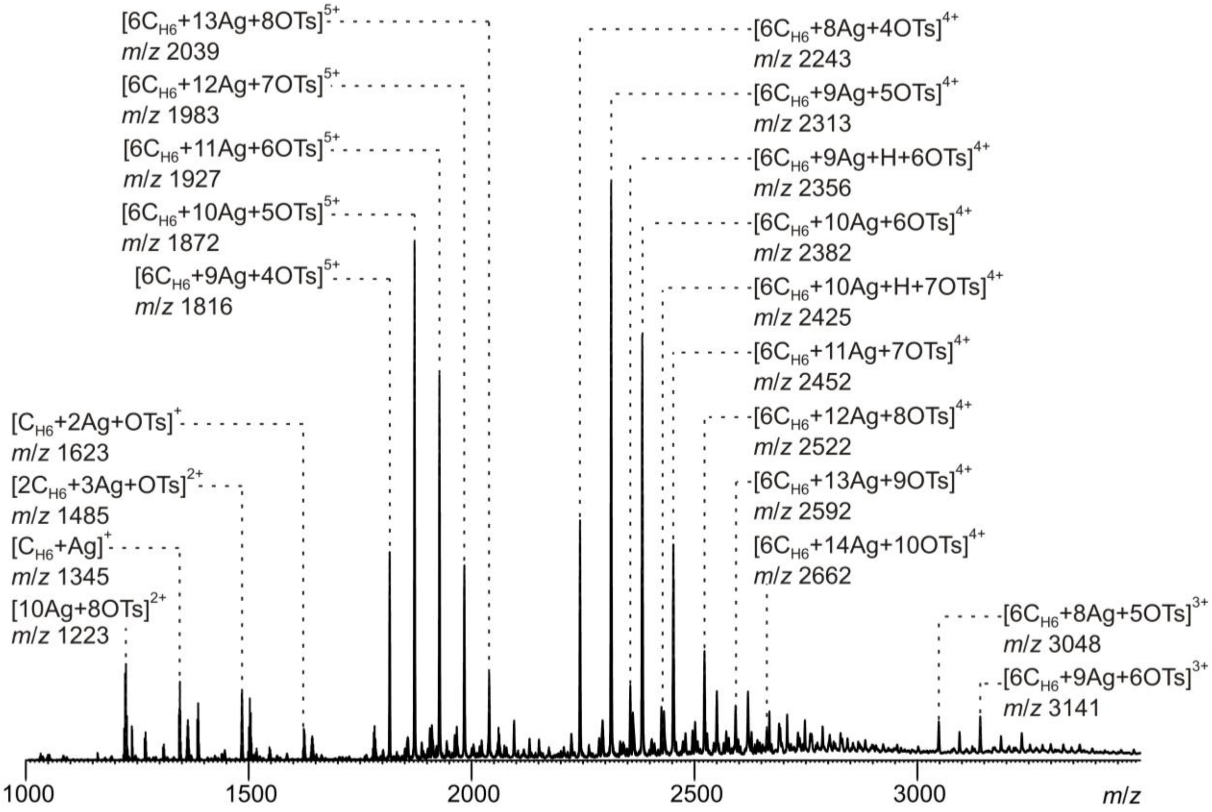

Figure S4: ESI-Q-TOF-HRMS spectrum of hexameric silver-coordinated capsule **4** (100 µM in CH_2Cl_2).

The solution exchange between preformed hexameric I^+-capsule **2** and free cavitand was examined by mixing a 1 mM solution of hexameric capsule **3** in $CHCl_3$ with 6 equivalents of a 1 mM solution of *iso*-butyl cavitand $\mathbf{C_{H4}}$. The mixed solution was diluted to 100 µM with $CHCl_3$ prior to the measurements and 10% of acetonitrile were added. Mass spectra were recorded after 2 minutes and after 20 hours equilibration time. No significant difference between these two spectra was observed. This experiment thus indicates that the exchange of the cavitands in the capsule occurs on a below-minutes time scales. No significant capsule dissociation occurs.

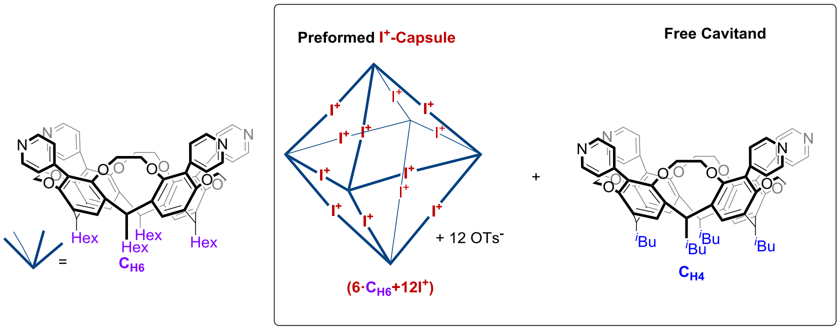

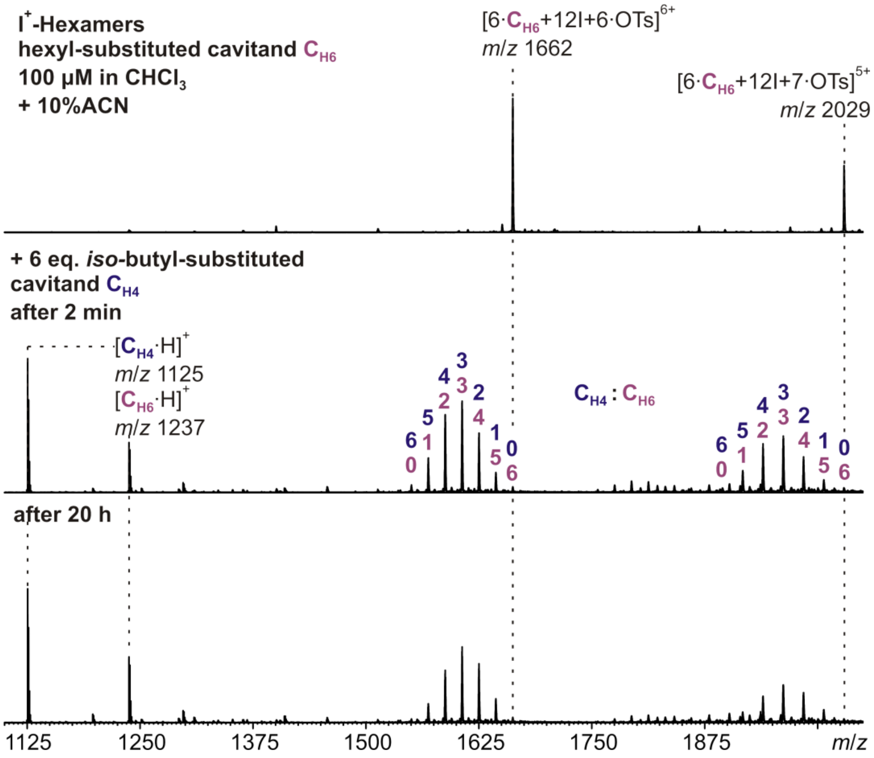

Figure S5: Mixing experiment hexameric capsule **2** and free *iso*-butyl cavitand $\mathbf{C_{H4}}$.

4. Tandem Mass Spectrometry

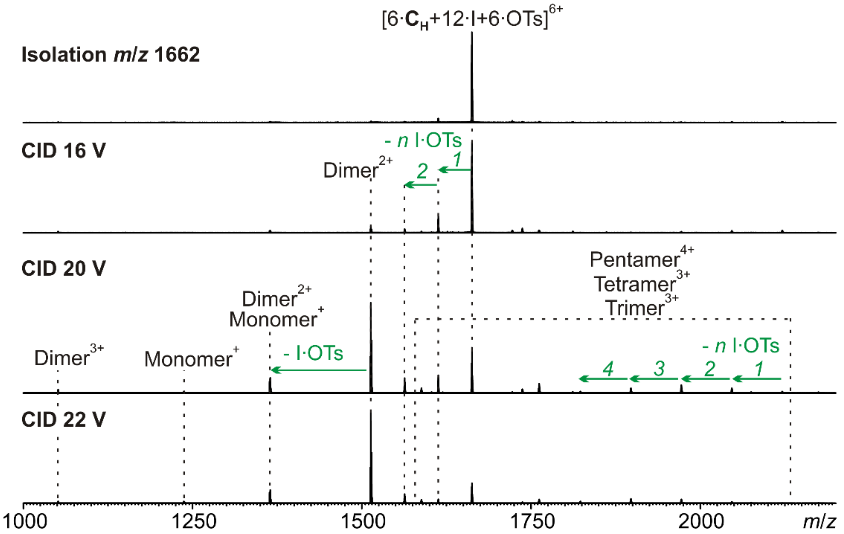

Figure S6: Tandem MS experiment performed with mass-selected ions $[6{\cdot}\mathbf{C_H}{+}12\mathrm{I}{+}6{\cdot}\mathrm{OTs}]^{6+}$ derived from the hexameric capsule **2**.

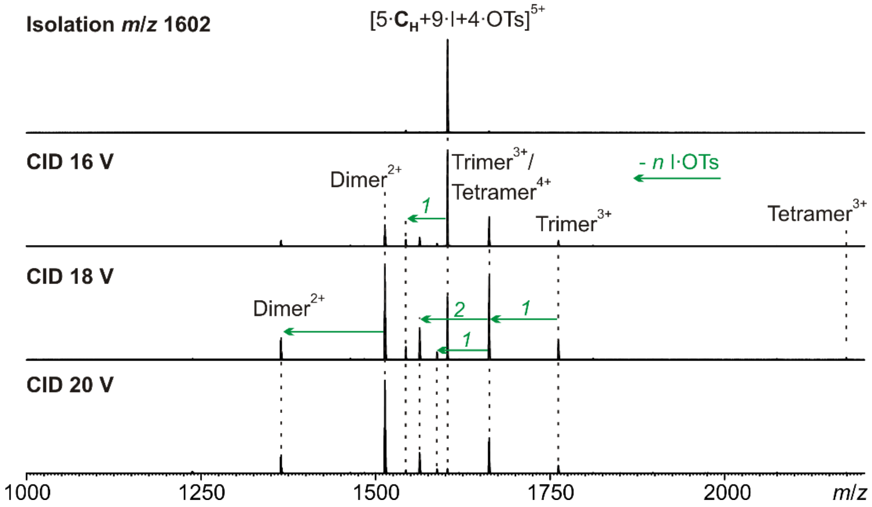

Figure S7: Tandem MS experiment performed with mass-selected ions $[5\cdot\mathbf{C_H}+9\mathrm{I}+4\cdot\mathrm{OTs}]^{5+}$ derived from the pentameric capsule **3**.

5. Theoretical calculations

Table S1. The difference between single point energies of MP2/def2-QZVPP and different density functional in kJ·mol^{-1}. The MP2/def2-TZVP optimized geometry of the [pyridine···I^{+}···pyridine] model system has been used for energy evaluation.

Functional	type	def2-SVP	def2-TZVP	def2-TZVPP	def2-QZVPP
TPSS	GGA	5.4	-2.1	-2.1	15.1
BLYP	GGA	-24.3	-47.3	-47.3	-48.1
PBE	GGA	14.2	1.7	1.7	33.9
PBE+D3	GGA	25.5	12.6	12.6	45.2
B3LYP	Hybrid	-38.9	-61.9	-61.9	-62.3
B3LYP+D3	Hybrid	-18.4	-41.4	-41.4	-41.8
PBE0	Hybrid	-8.8	-26.4	-26.4	-25.9
PBE0+D3	Hybrid	3.3	-14.2	-13.8	-13.4
M06	Hybrid	-38.9	-57.7	-56.5	-53.6
M06-2X	Hybrid	-49.8	-67.8	-68.2	-68.6
WB97-XD	Hybrid	-32.6	-52.3	-52.3	-51.5
X3LYP	Hybrid	-33.5	-56.5	-56.5	-56.9

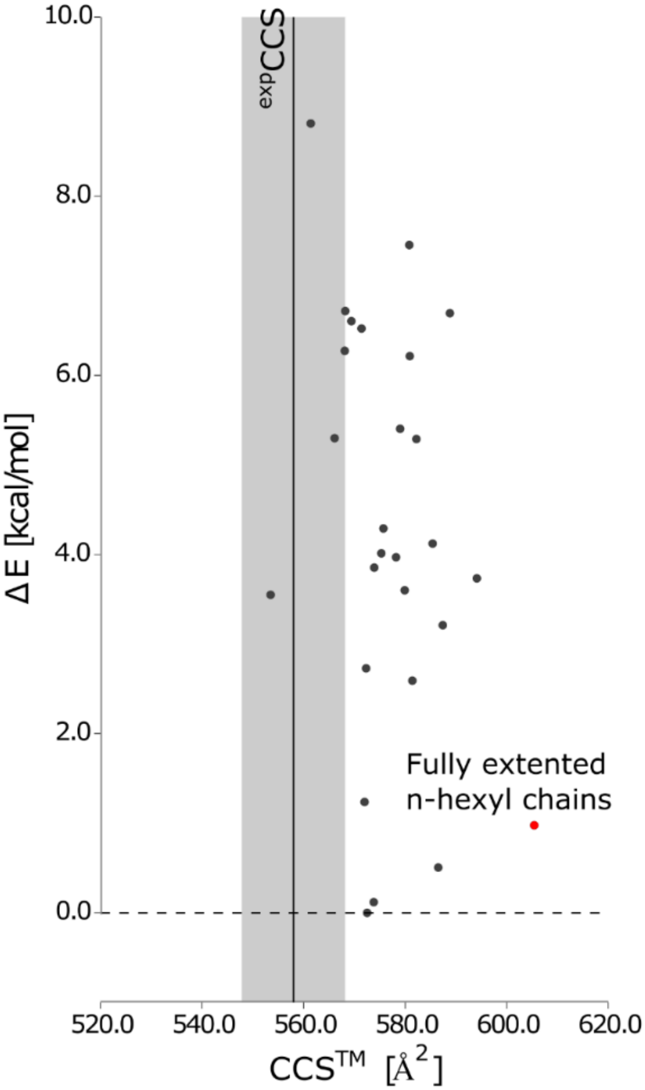

Figure S8: The distribution of CCS for the dimeric capsule **1** ([2$\mathbf{C_D}$+4I]$^{4+}$) computed for various conformations of *n*-hexyl chains using the trajectory method. The y-axis shows relative energies of optimized capsules. The fully extended chains give CCS larger that 600Å, whereas the chains can easily adopt more compact conformations.

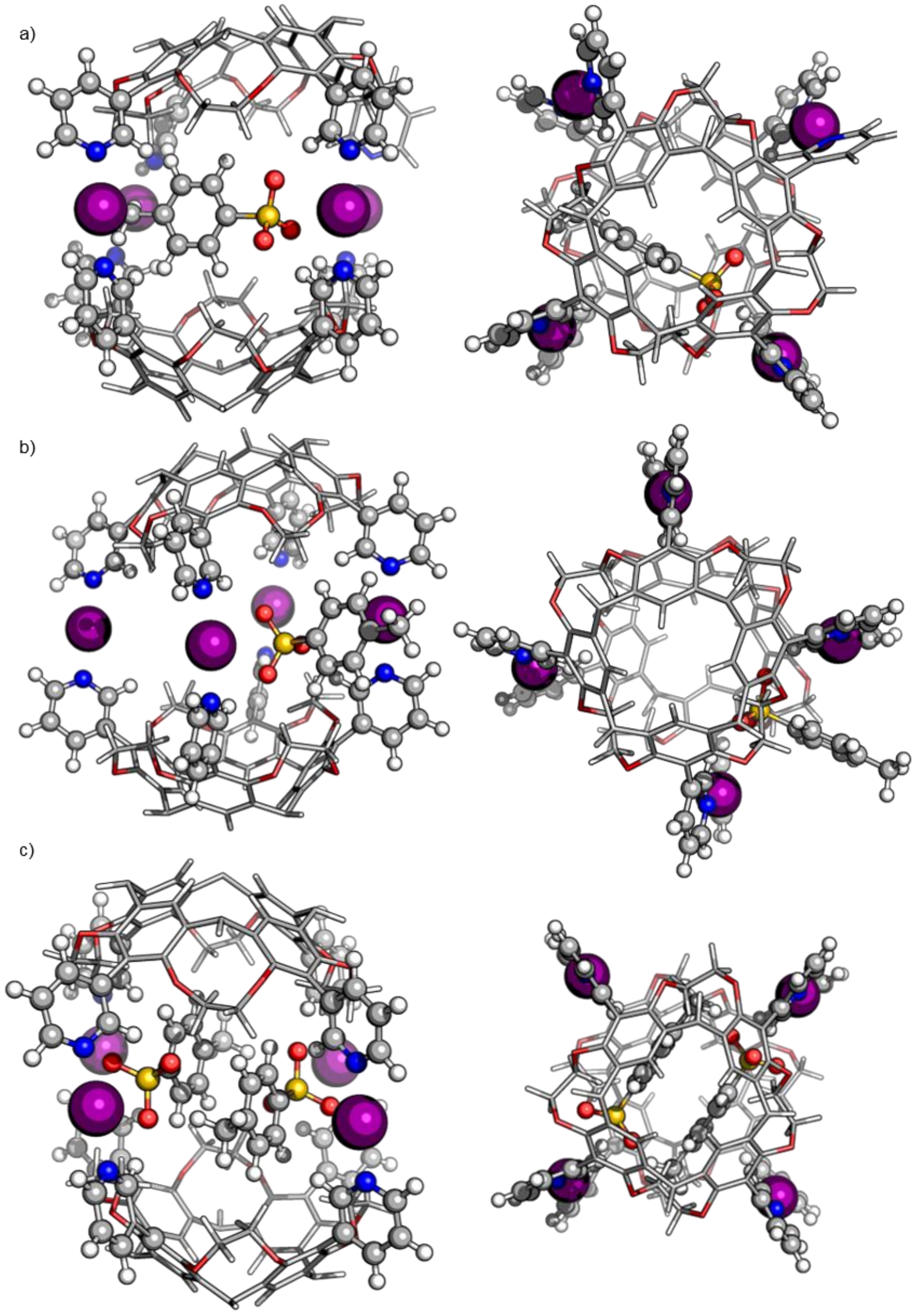

Figure S9: Calculated structures of dimeric halogen-bonded capsule **1** a) with one tosylate inside the cavity ($[2\cdot\mathbf{C}_\mathbf{D}+4\ \mathrm{I}+\cdot\mathrm{OTs}]^{3+}$), b) with one tosylate outside the cavity ($[2\cdot\mathbf{C}_\mathbf{D}+4\ \mathrm{I}+\cdot\mathrm{OTs}]^{3+}$) and c) with two tosylates inside the cavity ($[2\cdot\mathbf{C}_\mathbf{D}+4\mathrm{I}+2\cdot\mathrm{OTs}]^{4+}$). PBE0/def2-SVP was used for I^+, pyridines and tosylates (ball-and-stick representation); AM1 for cavitand (stick representation). For clarity, the *n*-hexyl side chains have been reduced to hydrogens in the image, but were included in the calculations.

6. References

[1] Turunen, L.; Warzok, U.; Puttreddy, R.; Beyeh, N. K.; Schalley, C. A.; Rissanen, K. *Angew. Chem. Int. Ed.* **2016**, *55*, 14033–14036.

[2] Turunen, L.; Warzok, U.; Schalley, C. A.; Rissanen, K. *Chem* **2017**, *3*, 861–869.